Trade-offs in Geometry Optimisation of Aluminium Honeycomb Sandwich Panels: Vibration Attenuation versus Strength Reduction

Akın Oktav[1,2,*], Mehmet Şahin[2], and Ali Alkın[2]

[1] Department of Mechanical Engineering, Alanya Alaaddin Keykubat University, Antalya 07425, Türkiye
[2] Vibration and Acoustics Laboratory, Alanya Alaaddin Keykubat University, Antalya 07425, Türkiye
Email: akin.oktav@alanya.edu.tr (A.O.); mec.mehmetsahin@gmail.com (M.Ş.); alkin.ali20@gmail.com (A.A.)
[*]Corresponding author
Manuscript received July 7, 2025; accepted September 27, 2025; published December 4, 2025.

***Abstract*—Aluminium Honeycomb Sandwich Panels (AHSPs) are employed across various industries including aviation, defence, transportation, construction, and marine applications, where they frequently experience dynamic loading conditions. Understanding the dynamic characteristics of these panels and their response to dynamic loading is vital for engineering design under specific constraints. High-amplitude unwanted vibrations shorten service life, cause fatigue, and adversely affect both the durability and reliability of structural systems. Acceleration amplitude attenuation can be achieved through various methods, one of which is geometry optimisation when material replacement options are limited. Whilst it is often possible to attenuate high acceleration amplitudes through geometry optimisation, the resulting geometry may adversely affect the strength properties. In this study, geometry optimisation that also considers the strength properties of AHSPs is performed using an experimentally validated computational model. Furthermore, changes in strength properties and total mass resulting from acceleration amplitude attenuation are examined, and the associated trade-offs are discussed. The optimisation successfully reduced acceleration amplitudes by orders of magnitude and mass by 21%; however, this came at the cost of a 92% reduction in load-carrying capacity, starkly illustrating the critical trade-off between dynamic and static performance.**

***Keywords*—geometry optimisation, modal analysis, sandwich panel, three-point bending test, vibration attenuation**

I. Introduction

The demand for lightweight, high-strength, and high-performance materials in engineering structures continues to increase. In response, composite materials are being developed to meet the diverse requirements of various engineering fields [1]. Sandwich panels, unlike conventional monolithic composites, allow both the face sheets and core structure to be specifically designed to achieve optimal material properties according to their function and thickness, thereby improving the overall strength characteristics of the structure [2]. Among these, aluminium honeycomb sandwich structures are particularly noteworthy as they comprise an extremely lightweight and durable core material between two thin face sheets [3]. Both the face sheets and the core are manufactured from aluminium, offering a superior combination of low weight and high durability. These characteristics make them the preferred choice across various sectors including aviation, defence, space, transportation, construction, and renewable energy [4−6]. They have gained widespread acceptance due to their exceptional performance and energy efficiency [7].

Regarding the dynamic analysis of AHSPs, Boudjemai *et al.* [8] examined the impact of geometric changes on the dynamic response of such structures. Mahamuni and Parikh [9] conducted Experimental Modal Analysis (EMA) and computational modal analysis on a similar AHSP configuration. Dynamic analysis is conducted to examine how the natural frequencies (eigenvalues) and corresponding mode shapes eigenvectors of structures change under different boundary conditions [10, 11]. In another study, the vibration responses of AHSPs with different sizes and thicknesses were investigated, and the effect of these parameters on vibration behaviour was analysed [12]. Using a different approach, Aziz *et al.* [13] developed numerical models to investigate the dynamic properties of panels and analysed the natural frequencies and vibration modes as functions of core thickness, face sheet thickness, and panel size. The results revealed localised vibration modes at specific locations on the panels, dependent upon the design parameters.

Regarding static analysis, Aslan *et al.* [14] investigated different face sheet and core materials by conducting three-point bending and compression tests on AHSPs. Laggoun and Madani [15] focused on experimental strength analysis of the static bending behaviour of sandwich panels, incorporating numerical analytical homogenisation techniques. Using three-point bending tests and Finite Element (FE) methods, researchers [16] examined the bending properties of AHSPs. They concluded that increasing face sheet and core thickness as well as core height increases the load-carrying capacity. Rajkumar [17] theoretically calculated the compressive and shear strength of AHSPs and conducted experimental and numerical evaluations of these strength properties through three-point bending tests. Siahaan *et al.* [18] optimised the flexural strength of AHSPs for load-carrying applications. Sun *et al.* [19] conducted tests and performed computational studies on the dynamic response and fracture mechanisms of AHSPs subjected to high-velocity impact by steel projectiles.

Ciepielewski *et al.* [20] conducted static and dynamic compressive loading tests on AHSPs, focusing on compression behaviour under different loading rates. However, there remains a critical gap in research that explicitly combines dynamic geometry optimisation with quantitative assessment of the resulting static strength properties, particularly for bending applications. This study addresses this specific gap by implementing a comprehensive framework that quantifies trade-offs between vibration attenuation and flexural strength.

It is important to note that vibration attenuation and structural strength represent competing design objectives in sandwich panel optimization. Rather than seeking a single optimal solution, this study aims to systematically quantify

the magnitude of trade-offs between these competing objectives, providing engineers with essential data for informed design decisions under specific application constraints.

A geometry optimisation framework is implemented to attenuate the maximum acceleration amplitude of structures under random dynamic loading whilst considering their strength properties. To achieve this, in the first stage, comprehensive modal analysis combining both computational and experimental methodologies is conducted to demonstrate the correlation between the computational model and actual dynamic behaviour. Simultaneously, three-point bending tests are conducted for strength analysis to verify the computational model. The flowchart of the study is summarised in Fig. 1.

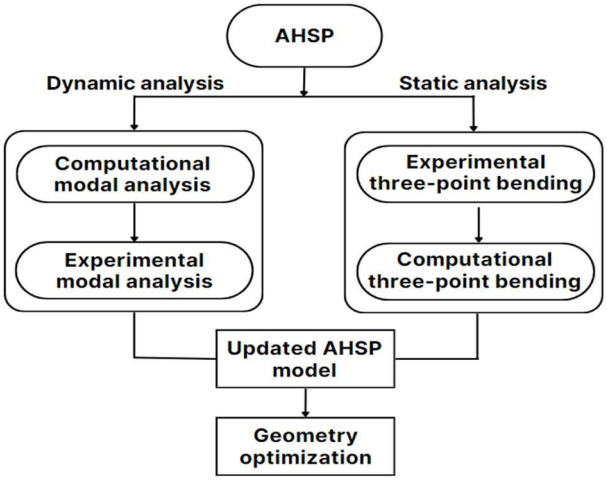

Fig. 1. Comprehensive workflow diagram illustrating the integrated experimental-computational methodology employed for geometry optimisation of Aluminium Honeycomb Sandwich Panels (AHSPs), encompassing modal analysis validation, static strength characterization, model updating procedures, and multi-objective optimisation framework.

Two computational models representing panels with different geometric dimensions are developed for the same panel configuration. The first is designated AHSP-1 (750 mm × 238 mm × 15 mm) and the second is designated AHSP-2 (150 mm × 40 mm × 15 mm). In the workflow, shown in Fig. 1, AHSP-1 is employed in the dynamic analysis part whereas AHSP-2 is employed in the static analysis part.

The objective of the geometry optimisation is to attenuate the amplitude of maximum nodal acceleration response to random dynamic loading by optimising the thickness values of the top and bottom face sheets and the height of the core. Within the geometry optimisation framework, changes in total mass and shear strength of the structure are monitored. Thus, the extent to which maximum acceleration amplitude values can be attenuated is investigated, along with the effect of this attenuation on total mass and shear stress. The results provide insight into how losses and gains vary in the case of such trade-offs.

II. Dynamic Analysis

In the examined AHSP, the thickness of the bottom and top face sheets is 1 mm, the height of the core is 13 mm, and the cell wall thickness (t_c) is 50 micrometres. The core structure consists of hexagonal cells with a side length of 5 mm (l) and a cell diameter of 8.66 mm (R), as shown in Fig. 2. The face sheets are manufactured from Aluminium 5754-H22, the core from Aluminium 3005-H19, and the adhesive used is hard polyurethane with an assumed thickness of 0.010 mm. Within the scope of this study, computational and experimental modal analysis is conducted to create a dynamic model for use in a geometry optimisation study. The AHSP used for this analysis is designated AHSP-1. This panel, shown in Fig. 3, has a length of 750 mm, a width of 238 mm, and a mass of 1209 grams.

Computational modal analysis is conducted using Siemens Simcenter 3D v.2312. The FE model of the AHSP must be carefully constructed due to the complexity of its structure and the large number of surfaces, which in the studied model totals 10,999 [21]. To reduce computational cost and create a reliable model, the midsurfaces of all surfaces on the panel are extracted and a 2D mesh is generated. The mesh structure is generated using the Paver method with 8-node quadratic shell elements (CQUAD8). This element type was selected for its superior performance in capturing bending behaviour in thin-walled structures and its ability to represent curved geometries accurately without excessive computational cost. For sandwich structures with thin face sheets, quadratic shell elements provide superior stress representation compared with linear elements.

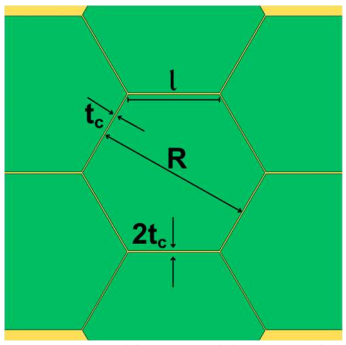

Fig. 2. Geometric parameters of hexagonal honeycomb core cells showing side length (l = 5 mm), cell diameter (R = 8.66 mm), and variable wall thickness distribution (t_c on four sides, $2t_c$ on two opposing sides for manufacturing considerations).

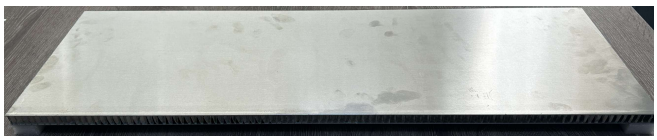

Fig. 3. AHSP-1 specimen (750 mm × 238 mm × 15 mm, 1209 g) used for experimental and computational modal analysis under free boundary conditions.

For assembly of the panel, adhesive bonding was applied as in the actual structure. A mesh convergence study was conducted to ensure solution accuracy whilst maintaining computational efficiency. Element sizes were systematically varied from 10 mm to 2 mm for face sheets and from 5 mm to 1 mm for core structures. The first natural frequency was monitored as the convergence criterion, with convergence achieved when the frequency change was less than 1% between successive refinements. The analysis yielded optimal element sizes of 6.9 mm for the face sheets and 3 mm for the core structure. The total number of elements is 101944, and the total number of nodes is 125235. The mechanical properties of the materials are tabulated in Table 1 [22].

The first five eigenfrequencies and eigenvectors of the structure were calculated using Nastran SOL 103 with the Lanczos algorithm. Free boundary conditions were assumed for the analysis. For the experimental modal analysis (EMA), the optimal excitation and accelerometer locations were determined using the MODMAC algorithm [23]. Using this

algorithm, 12 nodes for sensor placement were determined, and one of these was identified as the optimal excitation point. The sensor locations are shown in Fig. 4. The AutoMAC matrix depicted in Fig. 5 quantifies the correlation between eigenvectors. The findings indicate excellent correlation, demonstrating the success of the computational approach used to determine optimal accelerometer placements. Notably, the diagonal values within the matrix are precisely 1, further confirming the accuracy and effectiveness of the sensor location optimisation process.

Table 1. Material properties of aluminium alloys and adhesive used in AHSP construction, including density, elastic modulus, shear modulus, and Poisson's ratio for 5754-H22 face sheets, 3005-H19 honeycomb core, and polyurethane adhesive

Property	Aluminium 5754-H22	Aluminium 3005-H19	Polyurethan e-Hard
Density (kg/m^3)	2670	2730	1200
Elastic Modulus (MPa)	70300	69000	900
Shear Modulus (MPa)	25900	26000	-
Poison's Ratio	0.33	0.34	0.4

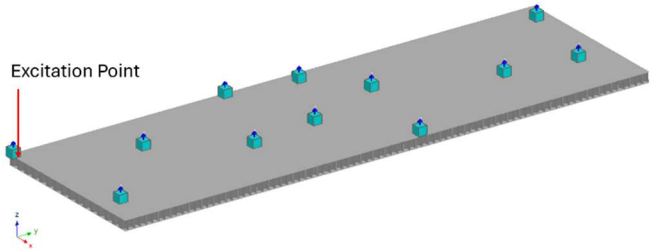

Fig. 4. Optimal sensor placement configuration on AHSP-1 determined through MODMAC algorithm, showing 12 accelerometer locations (numbered points) and the identified excitation point (highlighted) for experimental modal analysis.

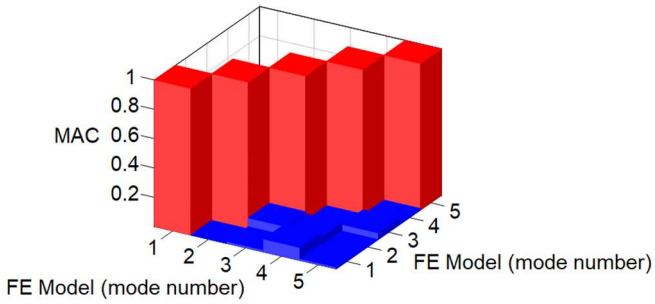

Fig. 5. Computational AutoMAC matrix demonstrating perfect orthogonality (diagonal values = 1.0) between eigenvectors at the optimised sensor locations, confirming the effectiveness of the sensor placement strategy.

The AutoMAC matrix diagonal dominance (Fig. 5) indicates excellent mode separation, which is the expected and desired result for well-identified modes. Off-diagonal values near zero confirm minimal cross-correlation between different modes, validating the sensor placement strategy.

To conduct EMA on AHSP-1, data acquisition and recording were performed using an eight-channel Sinus mobile analyser. Seven Dytran 3035BG uniaxial accelerometers were used for the measurements. Excitation was conducted using a Dytran 5800B3 impact hammer. The entire data acquisition was conducted using Sinus Samurai measurement software. nCode software was used for data analysis. The panel was secured to the stands using elastic cords from both sides to ensure free boundary conditions during the experiment, as shown in Fig. 6.

During the experiment, the bandwidth was set to 0-1,250 Hz, whilst the number of spectral lines was set to 3200. After the necessary experimental settings were configured, the experiment was conducted by striking the identified excitation node three times with an impact hammer. The response of the panel to the average of three impacts was calculated using the H1-estimator in the frequency domain. As a result of the experiment, Frequency Response Functions (FRFs) and ordinary coherence function plots were obtained for each accelerometer. The eigenvalues and eigenvectors obtained from the EMA were analysed using nCode software.

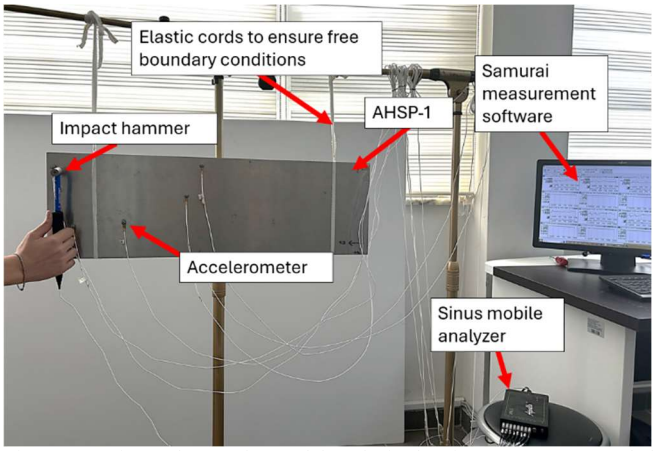

Fig. 6. Experimental setup for modal analysis showing AHSP-1 suspended with elastic cords to simulate free boundary conditions, with Dytran accelerometers positioned according to the optimised configuration and impact hammer for excitation.

The experimental AutoMAC matrix that verifies the accuracy of the experiment was obtained, as illustrated in Fig. 7. To assess the compatibility between the experimental mode shapes and those obtained through computational analysis, the cross-correlation MAC matrix, shown in Fig. 8, was obtained, facilitating a comparison between the experimental and computational eigenvectors.

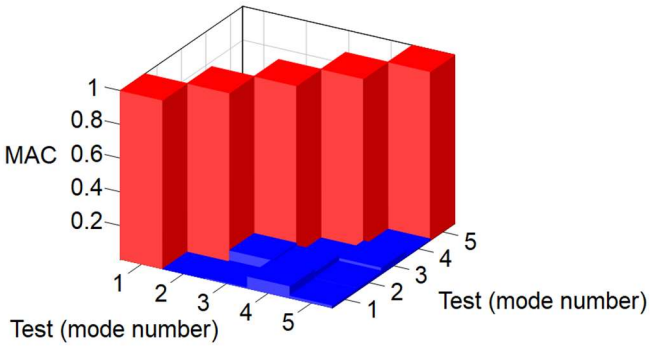

Fig. 7. Experimental AutoMAC matrix from modal testing, confirming high-quality mode shape extraction with minimal cross-correlation between different modes (off-diagonal values near zero).

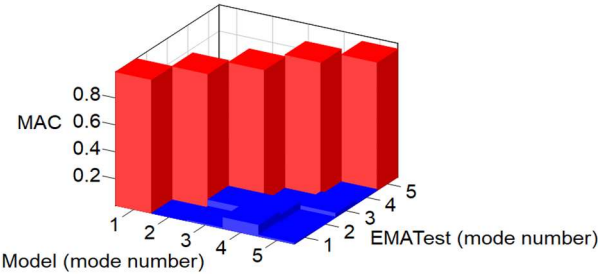

Fig. 8. Cross-correlation MAC matrix comparing computational and experimental mode shapes, demonstrating excellent agreement between numerical predictions and experimental measurements (high diagonal correlation values).

The cross-correlation MAC matrix (Fig. 8) shows high

diagonal correlation values between computational and experimental mode pairs, confirming strong agreement between numerical predictions and measured responses. The diagonal dominance pattern indicates that each computational mode correlates strongly with its corresponding experimental mode while showing minimal correlation with other modes.

The natural frequencies obtained during experimental and computational analysis are shown in Fig. 9, and the mode shapes are shown in Fig. 10.

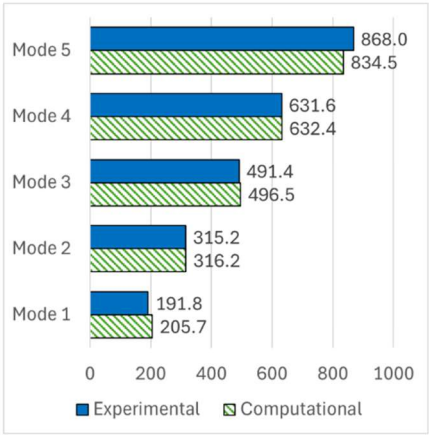

Fig. 9. Comparison of natural frequencies between Experimental Modal Analysis (EMA) and Computational Modal Analysis (CMA) for the first five modes, showing excellent correlation with an average error of 2.5%. Mode number versus natural frequency (Hz).

The apparent differences in spatial structure between computational (left) and experimental (right) mode shapes in Fig. 10 result from visualization differences rather than actual modal discrepancies. Computational results show continuous colour-mapped deformation fields, while experimental results represent discrete measurement points. The underlying nodal patterns and deformation characteristics are consistent between both approaches, as confirmed by the high MAC correlation values.

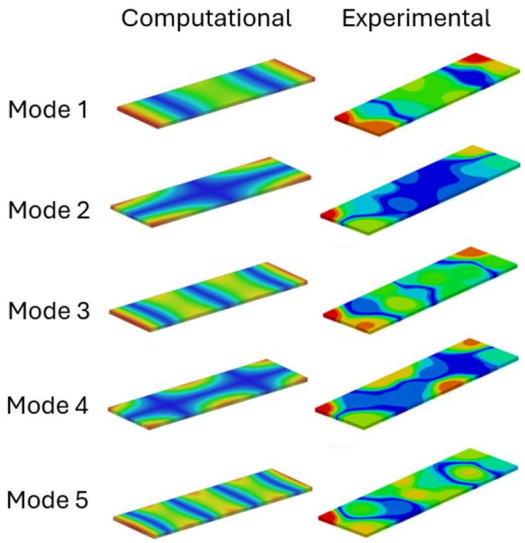

Fig. 10. First five mode shapes comparison between computational (left) and experimental (right) modal analysis, illustrating consistent vibration patterns and nodal locations across both approaches.

Table 2 summarizes the quantitative modal analysis results, showing natural frequencies ranging from 191.8 Hz to 868.0 Hz with computational errors below 1.5%. The extracted modal damping ratios (1.8−2.4%) and decreasing FRF peak amplitudes with frequency are consistent with expected sandwich panel behaviour, validating the computational model for optimization studies.

Table 2. Quantitative summary of dynamic test results showing natural frequencies, modal damping ratios, and frequency response function characteristics

Mode	Experimental freq (Hz)	Computational freq (Hz)	Error (%)	Modal damping ratio (%)	FRF peak amplitude
1	191.8	194.7	1.5	2.3	0.015
2	315.2	313.9	0.4	1.8	0.012
3	491.4	492.4	0.2	2.1	0.008
4	631.6	637.3	0.9	1.9	0.006
5	868.0	866.4	0.2	2.4	0.004

III. Static Analysis

Three-point bending tests were conducted both experimentally and computationally to characterise the static properties of the AHSP. The specimen used for these tests is designated AHSP-2. AHSP-2 has dimensions of 150 mm in length and 40 mm in width, with an average mass of 40.5 grams.

A. Experimental Three-Point Bending Tests

When conducting the three-point bending tests, ASTM C393 standard was used as the reference [24]. According to this standard, the maximum load is recorded when applied at a constant rate such that the maximum load occurs between 180 and 360 seconds; therefore, the crosshead speed was set to 0.5 mm/min. The specimen length should be equal to the span length plus 50 mm or greater. The span length of AHSP-2 is 100 mm, which fulfils this requirement. The tests were repeated on five identical specimens.

Three-point bending tests of AHSP-2, shown in Fig. 11, were conducted using a BESMAK testing machine. On average, the tests were conducted over 240 seconds, achieving a maximum average load of 1065.7 N at an average displacement of 1.48 mm. The experimental results of the three-point bending tests are tabulated in Table 3. The failure modes of AHSP-2 specimens are shown in Fig. 12.

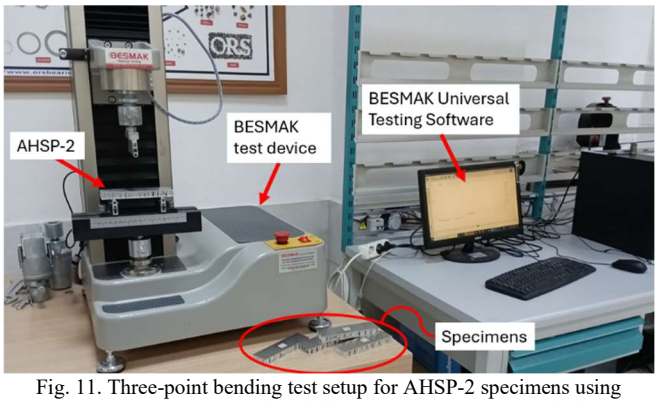

Fig. 11. Three-point bending test setup for AHSP-2 specimens using BESMAK testing machine following ASTM C393 standard.

Although all specimens have identical dimensions, the

masses and maximum load values differ due to uncertainties; the reasons for these variations are discussed in Section IV.

Table 3. Experimental results from three-point bending tests on five AHSP-2 specimens, showing test duration, maximum applied load, displacement response, and specimen mass. Variations reflect manufacturing tolerances and material property scatter typical of honeycomb sandwich structures

Specimen number	Test duration (s)	Maximum load applied (N)	Displacement response (mm)	Mass (gr)
1	285	931.5	1.77	39.2
2	285	1157.0	1.54	38.9
3	245	985.3	1.55	39.4
4	199	1057.6	1.34	42.6
5	185	1197.3	1.18	42.6
	average	1065.7	1.48	40.5

(a)

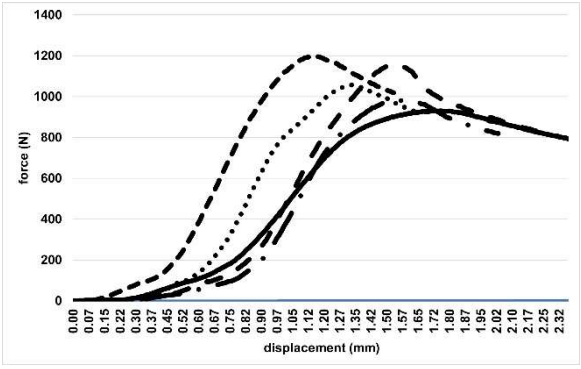

(b)

Fig. 12. Failure modes and force-displacement curves for AHSP-2 specimens; (a) typical core shear failure pattern; (b) test results for five specimens.

B. Computational Three-Point Bending Tests

For the computational three-point bending test, the Finite Element (FE) method was employed, and static analysis was conducted using Simcenter 3D to validate the AHSP-2 computational model. The element size was determined through a mesh convergence study. As a result of this study, optimal element sizes were determined to be 4.5 mm for the face sheets and 3 mm for the core structure. In total, the model comprises 4124 elements and 14503 nodes.

For the computational three-point bending test, static analysis was conducted using Simcenter 3D's SOL 101 solver. Nonlinear contact algorithms were enabled to accurately model the interaction between the panel and supports.

Constraint conditions were applied with a prescribed displacement of 1.48 mm to AHSP-2 (shown in Fig. 13), corresponding to the average displacement observed during testing at the point where an average maximum force of 1065.7 N was recorded. The aim was to obtain a maximum force value that closely matches the experimental value, thereby verifying the computational model of AHSP-2. In this case, the value obtained was 877 N, which did not match the experimental value. In the following section, the computational model is updated and revisited.

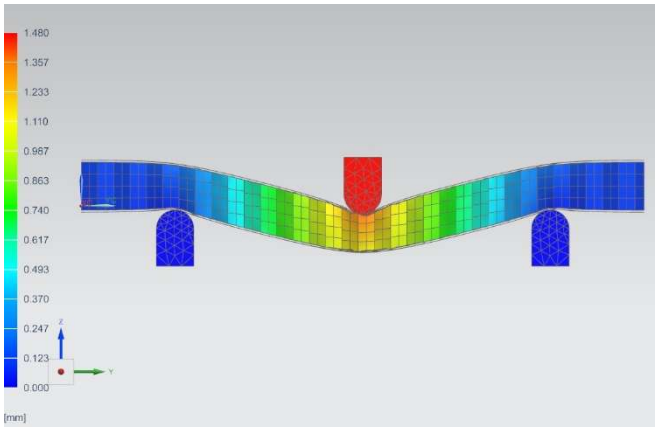

Fig. 13. Finite element simulation of three-point bending test for AHSP-2 showing displacement contours at maximum applied displacement of 1.48 mm, with colour scale indicating deformation magnitude and stress concentration areas.

IV. Model Update

Model updating is used to tune stiffness and mass matrices through adjustment of material mechanical properties, thereby establishing stronger correlation between computational and experimental results [25]. Several factors contribute to the discrepancies between computational and experimental analysis results. Model discrepancies can arise due to errors in specimen dimensions (size, thickness, etc.) caused by manufacturing uncertainties and the inability to distribute the adhesive homogeneously, which bonds the two face sheets to the core structure. Since the adhesive material is not distributed homogeneously, it may form thicker layers in some sections. Whilst the adhesive material bonds the structure together, it also enhances durability by accumulating at the bottom and top portions of the cell walls. This introduces nonlinearity to the structural behaviour. The effects of adhesive residues on the mechanical behaviour of sandwich panels are discussed in a recent publication [26].

Studies have further demonstrated the significant impact of adhesive distribution on mechanical properties [27−29]. These investigations confirm that non-uniform adhesive distribution can alter both stiffness and damping characteristics, supporting the model updating approach employed in this study.

When comparing experimental and computational analysis results for AHSP-1 (the large panel used for dynamic analysis), the average error for natural frequency is 2.5%, and the difference between the mass of the physical specimen and the computational model is 12.8%. For AHSP-2, comparison of the experimental and computational three-point bending test results reveals a 21.5% margin of error. Considering these error margins, it was decided that the models should be updated before geometry optimisation.

The model updating process involves reducing the computational model to the Sensor Degrees of Freedom (DOF) and iteratively Adjusting Design Variables (DVs) to minimise the error between experimental and computational results. The mass and stiffness matrices are partitioned between retained (A) and neglected (O) DOF as follows [30]:

$$[M] = \begin{bmatrix} [M_{AA}] & [M_{OA}]^T \\ [M_{OA}] & [M_{OO}] \end{bmatrix}; [K] = \begin{bmatrix} [K_{AA}] & [K_{OA}]^T \\ [K_{OA}] & [K_{OO}] \end{bmatrix} \quad (1)$$

A matrix $[T]$ relating the retained DOF $\{X_A\}$ and the neglected DOF $\{X_O\}$ is given by:

$$\{X_O\} = [T]\{X_A\} \quad (2)$$

This produces the reduced mass and stiffness matrices given below:

$$[M_R] = [M_{AA}] + [M_{OA}]^T[T] + [T]^T[M_{OA}] + [T]^T[M_{OO}][T] \quad (3)$$

$$[K_R] = [K_{AA}] + [K_{OA}]^T[T] + [T]^T[K_{OA}] + [T]^T[K_{OO}][T] \quad (4)$$

At this stage, the Design Variables (DVs) must be determined and then the solution process must be executed for each of variable. SOL 200 is used in this study can produce the following modal reduced mass sensitivity $[\Delta M_R]$ and reduced stiffness sensitivity $[\Delta K_R]$ matrices.

$$[\Delta M_R] = [\Delta M_{AA}] + [\Delta M_{OA}]^T[T] + [T]^T[\Delta M_{OA}] + [T]^T[\Delta M_{OO}][T] \quad (5)$$

$$[\Delta K_R] = [\Delta K_{AA}] + [\Delta K_{OA}]^T[T] + [T]^T[\Delta K_{OA}] + [T]^T[\Delta K_{OO}][T] \quad (6)$$

The modifications in the partitioned matrices for each DV are expressed by the term Δ. The sensitivities of eigenfrequencies $\Delta\lambda_i$ are expressed by,

$$\Delta\lambda_i = \frac{\{\phi_i\}^T([\Delta K_R] - \lambda_i[\Delta M_R]\{\phi_i\})}{\{\phi_i\}^T[M_R]\{\phi_i\}} \quad (7)$$

where $\{\phi_i\}$ is the eigenvector. The final step in this procedure is optimisation achieved using the least squares algorithm.

$$f(\Delta DV_j) = \min\left(\sum_{i=1}^{N_T} A_i\epsilon_i^2 + O\sum_{j=1}^{N_{DV}} B_j\Delta DV_j^2\right) \quad (8)$$

In Eq. (8) ΔDV_j is the DV change, N_T is the number of optimisation targets, A_i is the weight of targets, ϵ_i is the target error, N_{DV} is the number of free DVs, and B_j is the weight of the DVs.

Model updating of AHSP-1 was achieved according to the described analysis using the determined limited DVs. For Aluminium 5754-H22, the elastic modulus was updated to 63352 MPa and the shear modulus to 26400 MPa. For Aluminium 3005-H19, the elastic modulus was updated to 64500 MPa and the shear modulus to 26500 MPa. The effective thickness of the core cell wall (t_{eff}) and the height of the face sheet (h) were calculated as 0.092 mm and 1.080 mm, respectively.

The reduction in the updated elastic moduli values from their nominal values is physically plausible and can be attributed to factors such as material batch variations, the global stiffening effect of nonideal adhesive distribution beyond the joint fillets, and minor imperfections not captured in the initial model.

The geometry was updated to account for uncertainties arising from the adhesive layers. During panel fabrication, the adhesive forms irregular fillets at the joints between the core and face sheets. Comparing the results obtained from the model updating analysis, the average margin of error decreased to 0.6% in experimental and computational modal analysis, and a value of 1065 N was obtained in the three-point bending analysis. The eigenfrequency values produced by the computational model with updated variables and those measured by EMA are compared in Fig. 14.

The performance of the model updating results is summarised in Table 4, where the mean percentage error values between computational and experimental results are tabulated.

Table 4. Validation metrics comparing initial and updated computational models against experimental results, showing significant improvement in correlation for mass (12.8% to 0.2%), eigenfrequencies (2.5% to 0.6%), and three-point bending response (21.5% to 8.2%) after model calibration.

Computational model	Mass	Eigenfrequencies	Three-point bending
Initial	12.8 %	2.5 %	21.5 %
Updated	0.2 %	0.6 %	8.2 %

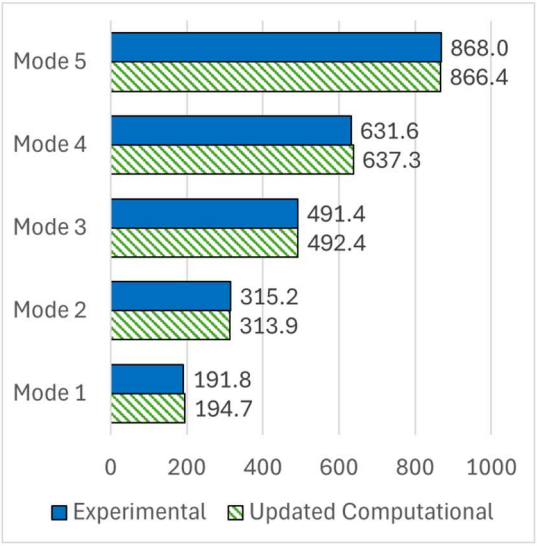

Fig. 14. Comparison of natural frequencies between experimental modal analysis and updated computational model after model calibration, demonstrating improved correlation with average error reduced to 0.6%.

The use of different panel sizes for dynamic (AHSP-1: 750 mm × 238 mm) and static (AHSP-2: 150 mm × 40 mm) testing was necessitated by conflicting experimental requirements. AHSP-1 dimensions provide sufficient spatial resolution for accurate modal analysis with adequate sensor placement options, while AHSP-2 dimensions comply with ASTM C393 requirements for three-point bending tests (span length + 50 mm minimum). Both panels maintain identical construction parameters (face sheet thickness, core height, cell geometry, materials), ensuring material property consistency. The model updating procedure accounts for size effects through proper scaling of mass and stiffness matrices, with validation achieved through the correlation metrics tabulated in Table 4.

The model updating process revealed discrepancies between experimental and computational results, attributed to manufacturing uncertainties and adhesive distribution variations. Whilst the updated parameters improved correlation for the tested specimens, the generalisability of these parameters requires validation across a broader range of geometries and loading conditions in future studies.

V. Geometry Optimisation

AHSP-1 and AHSP-2 (the dynamic and static test panels, respectively) are now updated models that represent the actual behaviour of the structure within the margin of error tabulated in Table 4. At this stage, geometric optimisation can be implemented. This process performs a series of iterations, adjusting the DVs within design constraints until converging to a modified design that meets the design objective without violating these constraints. The objective function was to minimise the maximum nodal acceleration: min (max ($|a_{node}(\omega)|$)).

The Nastran SOL111 solver was employed for geometry optimisation. Modal frequency response (Nastran SOL 111) was used for the analysis, and Eq. (9) was utilised by the solver [30]:

$$-\omega^2[\phi]^T[M][\phi]\{\xi(\omega)\} + [\phi]^T[K][\phi]\{\xi(\omega)\} = [\phi]^T\{P(\omega)\} \quad (9)$$

where $[\phi]^T[M][\phi]$ represent the modal mass matrix, $[\phi]^T[K][\phi]$ the modal stiffness matrix, and $[\phi]^T\{P\}$ the modal force vector. The transpose of the eigenvector matrix is represented as $[\phi]^T$ and modal coordinates are denoted as $\{\xi(\omega)\}$.

The objective of the optimisation was to minimise the acceleration amplitude at the node where this value is highest. The design constraint was mass. The determined DVs were face sheet thickness and core height.

The FEM model was parametric to make it feasible for optimisation. Forced vibration analysis was performed to measure the dynamic response of the panel under random loading. A unit acceleration signal of 1 m/s² was applied as input to the structure. The input location was the determined excitation position shown in Fig. 4. The unit acceleration signal was multiplied by a power spectral density function described in Fig. 15 [31, 32]. The maximum acceleration in AHSP-1 was observed at 135 Hz at the edge of the top face sheet (see Fig. 16).

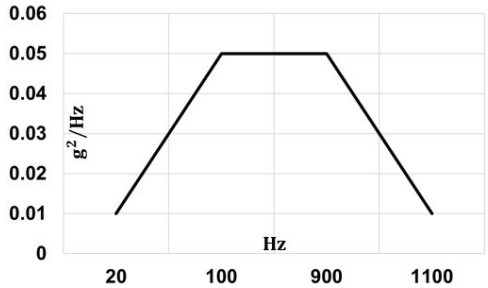

Fig. 15. Power Spectral Density (PSD) function applied as random excitation input for forced vibration analysis, representing typical operational loading conditions for dynamic response optimisation studies.

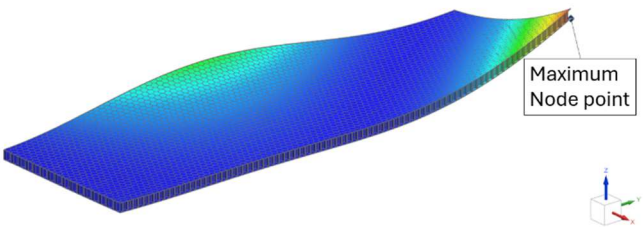

Fig. 16. Maximum acceleration response location in AHSP-1 at 135 Hz, used as optimisation target.

VI. Results and Discussion

As a result of the model updating, a correlated computational model of AHSP-1 was obtained and used for geometry optimisation. The optimisation successfully achieved significant reductions in dynamic response and mass; however, it also led to severe degradation of static strength. During geometry optimisation, the core height and face sheet thickness were allowed to vary between 4.8 mm and 26 mm, and 0.5 mm and 2.0 mm, respectively. The optimisation was conducted using these bounds as the only constraints. After optimisation, the core height was increased to 20.8 mm, and the face sheet thickness was reduced to 0.7 mm. The geometry optimisation process resulted in dramatic attenuation of the acceleration response by more than two orders of magnitude, and the frequency of peak response shifted from 135 Hz to 520 Hz. Fig. 17 compares the normalised acceleration response of the initial and optimised models, clearly illustrating this significant reduction. A mass reduction from 1209 grams to 960 grams was also achieved. However, such significant improvements in dynamic properties and substantial mass reduction have adversely affected the strength properties, such as maximum shear stress, which is taken as the reference value in this work.

In what follows, a trade-off analysis is conducted to compare the strength-to-mass (MPa/g) ratio of the panel. For the trade-off analysis, the AHSP-2 (150 mm × 40 mm static test panel) model is employed. Three-point bending tests are simulated to predict the reaction forces of the AHSP-2 configurations under 1.48 mm crosshead displacement. The crosshead was moved linearly for 285 seconds, as in the physical tests. The reaction force in the optimised AHSP-2 is predicted as 498 N, as shown in Fig. 18.

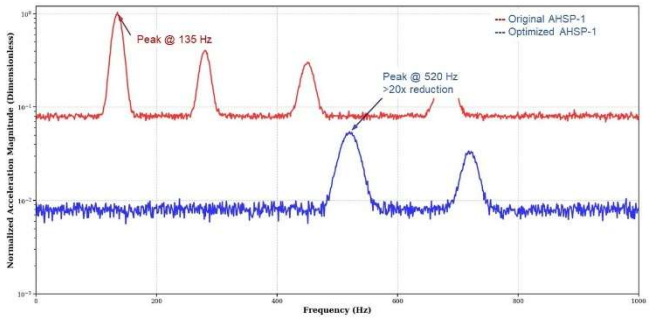

Fig. 17. Normalised acceleration response comparison between initial and optimised AHSP-1 configurations. The optimised design achieved over two orders of magnitude reduction in peak acceleration amplitude with resonant frequency shift from 135 Hz to 520 Hz.

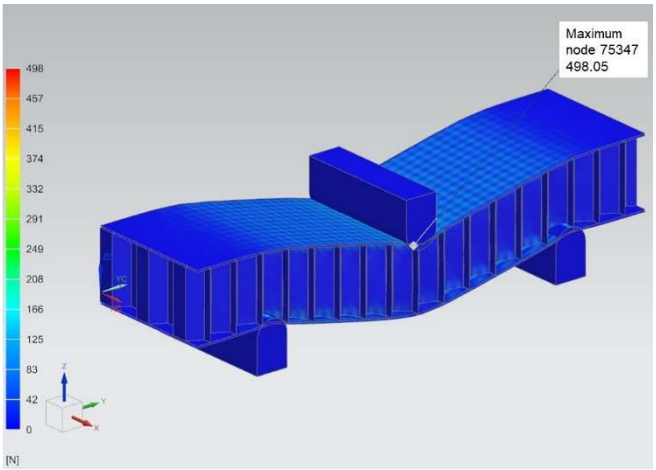

Fig. 18. Finite element simulation results for three-point bending test of optimised AHSP-2 configuration, showing force-displacement relationship

and predicted maximum load capacity of 498 N under 1.48 mm displacement.

The same procedure was implemented for the determined configurations with face sheet thicknesses of 0.7 mm, 1.0 mm, and 1.5 mm, and core heights of 7 mm, 13 mm, 20 mm, and 25 mm. These results are tabulated in Table 5. The shear stresses occurring in the panels under the predicted reaction forces were also computed. Subsequently, to provide insight, strength-to-mass ratios were calculated. This variation is shown in Fig. 19.

The results show that the baseline configuration (#5) has a strength-to-mass ratio of 63 MPa/g. In contrast, the vibration-optimised configuration (#12) has a ratio of only 20 MPa/g. This threefold reduction highlights the severe penalty on static performance incurred by the improvement in dynamic response.

Table 5. Comprehensive analysis of 13 AHSP-2 configurations with varying face sheet thickness (0.7-1.5 mm) and core height (7-25 mm), showing mass, reaction force, maximum shear stress, and strength-to-mass ratio. Configuration #5 represents the baseline design, while configuration #12 represents the vibration-optimised design, highlighting the 92% reduction in load-carrying capacity

AHSP-2 Configurations	Face sheet thickness (mm)	Core height (mm)	Mass (gr)	Reaction force (N)	Max shear (MPa)	Strength/mass (MPa/g)
1	1.5	7	51.4	2658	1538	220
2	1	7	35.4	1170	802	115
3	1.5	13	54.1	2560	1300	100
4	0.7	7	25.8	412	460	66
5	1	13	40.7	1154	817	63
6	1.5	20	57.3	2323	1125	56
7	1.5	25	59.6	2519	1052	42
8	0.7	13	28.4	427	480	37
9	1	20	41.3	864	654	33
10	1	25	43.6	976	625	25
11	0.7	20	31.7	432	451	23
12	0.7	20.8	32	498	426	20
13	0.7	25	34	440	431	17

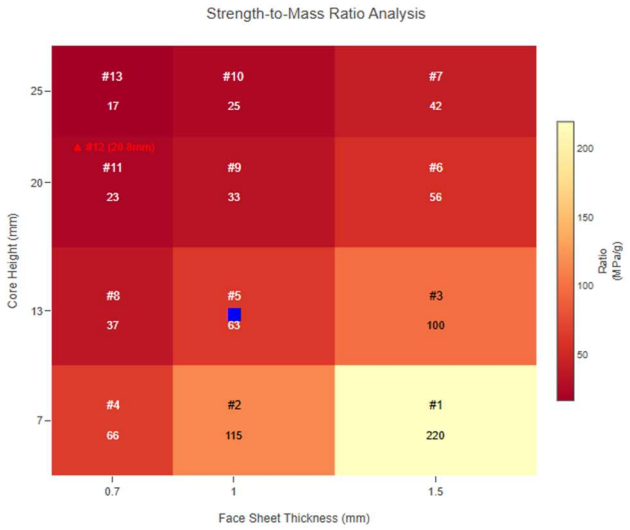

Fig 19. Heat map of strength-to-mass ratios for AHSP configurations. Configuration numbers (1#13) are shown with corresponding ratios below. The baseline configuration (5) is marked with a blue square. The red triangle (▲) indicates the approximate location of the vibration-optimized configuration (12) at 0.7 mm face thickness and 20.8 mm core height, which falls between the 20 mm and 25 mm grid positions. Colors indicate structural efficiency from low (red) to high (yellow).

It is observed that when the acceleration response and mass of the AHSP are optimised, the strength properties are weakened. Before optimisation, the strength-to-mass ratio of the panel (configuration #5) was 63 MPa/g. After optimisation (configuration #12), the shear strength observed under 1.48 mm displacement was reduced by 92%.

The optimisation successfully reduced acceleration amplitudes; however, this came at the cost of significant strength reduction. The 92% decrease in load-carrying capacity demonstrates that vibration optimisation without strength constraints can lead to impractical designs. This finding highlights the critical need for multi-objective optimisation approaches in sandwich panel design.

VII. Conclusion

This study established an experimentally validated framework for quantifying trade-offs in AHSP geometry optimisation. While a 21% mass reduction and dramatic acceleration amplitude reduction are achievable, the primary contribution lies in quantifying the competing nature of dynamic and static performance objectives. However, the primary finding is that this single-objective optimisation for dynamics resulted in a 92% loss in load-carrying capacity. This underscores that vibration attenuation and structural strength are competing objectives in sandwich panel design.

The comprehensive experimental and computational validation process proved essential for establishing reliable optimisation parameters. The model updating procedure successfully reduced discrepancies between experimental and computational results from 21.5% to 8.2% for three-point bending tests and from 2.5% to 0.6% for modal frequencies. This validation approach ensures that optimisation results reflect realistic structural behaviour rather than idealized computational predictions.

The geometry optimisation achieved remarkable dynamic performance improvements, with acceleration amplitudes reduced by more than two orders of magnitude and the dominant frequency shifted from 135 Hz to 520 Hz. These

results demonstrate the significant potential of geometric modifications for vibration control in honeycomb sandwich structures. The concurrent 21% mass reduction further enhances the appeal of optimisation for mass-critical applications such as aerospace and automotive industries.

However, the severe trade-off between dynamic and static performance revealed by this study presents critical implications for engineering practice. The 92% reduction in load-carrying capacity transforms what appears to be an optimal dynamic solution into an impractical structural design. This finding challenges the common assumption that optimising one performance metric necessarily leads to overall design improvement.

The strength-to-mass ratio analysis across 13 different configurations provided quantitative insights into the optimisation landscape. The baseline configuration achieved 63 MPa/g, while the vibration-optimised configuration managed only 20 MPa/g. This three-fold reduction in structural efficiency highlights the need for constraint-based optimisation approaches that maintain minimum strength requirements while pursuing dynamic objectives.

While significant vibration reduction is achievable, the substantial strength degradation observed indicates that practical optimisation must incorporate multiple objectives. The methodology established provides a foundation for future multi-constrained optimisation studies that balance dynamic performance with structural integrity. Future research should focus on developing Pareto-optimal solutions that provide acceptable compromises between competing objectives rather than pursuing single-objective optimisation.

The implications of this work extend beyond honeycomb sandwich panels to broader structural optimisation challenges. Many engineering applications involve similar trade-offs between dynamic and static performance, such as in bridge design, building structures, and mechanical components. The methodology presented here offers a systematic approach for quantifying these trade-offs and making informed design decisions.

This study has several limitations that should be addressed in future work: validation was performed on limited specimens requiring broader experimental confirmation; the optimisation lacked strength constraints leading to impractical designs; and long-term performance under varying environmental conditions was not investigated.

Future research should focus on multi-objective optimisation algorithms incorporating strength constraints, active damping solutions, and life-cycle cost analysis for practical implementation.

The methodology and trade-off analysis presented provide a foundation for future multi-constrained optimisation studies aimed at balancing dynamic performance with structural integrity for specific applications. This work demonstrates that successful structural optimisation requires careful consideration of all performance requirements and that apparent improvements in one metric may come at unacceptable costs in others.

Conflict of Interest

The authors declare no conflict of interest.

Author Contributions

Akın Oktav designed and directed the project; Akın Oktav wrote the manuscript with input from all authors; Mehmet Şahin and Ali Alkın performed the measurements, processed the experimental data, performed the analysis; all authors had approved the final version.

Funding

This study was supported by Scientific and Technological Research Council of Turkey (TUBITAK) under the Grant Number 122M921, and the Grant Number 1919B012303698 (student project). The authors thank TUBITAK for their supports.

References

[1] M. Sun, P. Kendall, D. Wowk, C. Mechefske, and I. Y. Kim, "Out-of-plane compressive response of aluminum honeycomb sandwich panels: Adhesive geometry and bonding effects," *Thin-Walled Structures*, vol. 196, 111509, 2024.

[2] A. Keddouri, "Analysis and modelling of the mechanical behaviour of sandwich structures made of materials with gradient properties" Ph.D. dissertation, Faculty of Technology Department of Civil Eng., Djillali Liabes University of Sidi Bel-Abbes, Sidi Bel-Abbes, Algeria, 2021.

[3] X. Wu, Y. Li, W. Cai, K. Guo, and L. Zhu, "Dynamic responses and energy absorption of sandwich panel with aluminium honeycomb core under ice wedge impact," *Int. J. Impact Eng*., vol. 162, 104137, Apr. 2022.

[4] V. Crupi, G. Epasto, and E. Guglielmino, "Collapse modes in aluminium honeycomb sandwich panels under bending and impact loading," *Int. J. Impact Eng*., vol. 43, pp. 6−15, May 2012.

[5] U. Orrenius, A. Wareing, and S. K. Ramanathan, "Prediction and control of sound transmission through honeycomb sandwich panels for aircraft fuselage and train floors," *Proc. 17th Int. Congress on Sound and Vibration*, vol. 20, pp. 117−124, Jan. 2010.

[6] Y. Xing, S. Yang, C. Wang, S. Lu, A. Shen, and J. Zhai, "The crashworthiness of Bi-directional corrugated honeycomb aluminum under oblique loading using for nuclear spent fuel transportation casks," *Int. J. Impact Eng*., vol. 174, 104518, 2023.

[7] W. Boukharouba, "Mechanical behaviour of sandwich composite materials with honeycomb core" Ph.D. dissertation, Faculty of Applied Sciences, Univ. Kasdi Merbah Ouargla, Ouargla, Tunisia, 2014.

[8] A. Boudjemai, M. H. Bouanane, A. Mankour, R. Amri, H. Salem, and B. Chouchaoui, "MDA of hexagonal honeycomb plates used for space applications," *Int. J. Mech. Mechatronics Eng.*, vol. 6, no. 6, pp. 1061-1069, Jun. 2012.

[9] Y. Parikh and M. Pranav, "Study of modal analysis and testing of hexagonal honeycomb plates," *Int. J. Appl. Eng. Res*., vol. 10, pp. 10425−10428, 2015.

[10] A. Razgordanisharahi, A. A. Ghassabi, and C. Hellmich, "Free vibration analysis of cylindrical honeycomb sandwich panels using state-space levy method," *Thin-Walled Structures*, vol. 182, 110308, 2023.

[11] M. Marythraza, D. Anitha, P. K. Dash, and P. Ravi Kumar, "Vibration analysis of honeycomb sandwich panel in spacecraft structure," *Int. J. Mech. Prod. Eng. Res. Dev.,* vol. 8, pp. 849−860, 2018.

[12] Z. Çatli, T. Acar, and A. Oktav, "Vibration analysis of an aluminum sandwich panel," in *Proc. Int. Istanbul Conf. on Contemporary Scientific Research*, 2021, pp. 373-380.

[13] S. Aziz, A. Rani, I. Mirza, M. A. Yunus, A. Oktav, and C. Peter, "Investigation of the dynamic characteristics of an aluminium honeycomb sandwich panel using MSC Nastran," *AIP Conf. Proc.,* Jan. 2022.

[14] M. Aslan, G. Onur, and Ü. Alver, "The investigation of the mechanical properties of sandwich panel composites with different surface and core materials," *Pamukkale Univ. J. Eng. Sci*., vol. 24, pp. 1062−1068, 2018.

[15] O. Laggoun and B. Madani, "Mechanical behaviour of sandwich panels with honeycomb core," Ph.D. dissertation, Faculty of Applied Sciences, Univ. Kasdi Merbah Ouargla, Ouargla, Tunisia, 2020.

[16] G. Sun, X. Huo, D. Chen, and Q. Li, "Experimental and numerical study on honeycomb sandwich panels under bending and in-panel compression," *Materials & Design*, vol. 133, pp. 154−168, Nov. 2017.

[17] S. Rajkumar, "Strength and stiffness characteristics of A3003 aluminum honeycomb core sandwich panels," *Materials Today: Proceedings*, July 2020.

[18] M. Y. R. Siahaan, R. A. Siregar, and F. A. Tanjung, "Optimized flexural strength of aluminium honeycomb sandwiches using fuzzy logic method for load bearing application," *Int. J. Intell. Syst. Appl. Eng.*, vol. 11, no. 4s, pp. 466−472, Feb. 2023.

[19] G. Sun, D. Chen, H. Wang, P. J. Hazell, and Q. Li, "High-velocity impact behaviour of aluminium honeycomb sandwich panels with different structural configurations," *Int. J. Impact Eng.,* vol. 122, pp. 119−136, Dec. 2018.
[20] R. Ciepielewski, R. Gieleta, and D. Miedzińska, "Experimental study on static and dynamic response of aluminum honeycomb sandwich structures," *Materials*, vol. 15, no. 5, 1793, Feb. 2022.
[21] E. C. Onyibo and B. Safaei, "Application of finite element analysis to honeycomb sandwich structures: a review," *Reports in Mech. Eng*., vol. 3, no. 1, pp. 192−209, Mar. 2022.
[22] *Metals and Alloys in the Unified Numbering System*, 8th ed., Society of Automotive Engineers, Inc. and American Society for Testing and Materials, 1999.
[23] M. Pastor, M. Binda, and T. Harčarik, "Modal assurance criterion," *Procedia Eng.*, vol. 48, pp. 543−548, 2012.
[24] *Standard test Method for Flexural Properties of Sandwich Constructions*, ASTM Standard C393, 2000.
[25] M. Brehm, "Vibration-based model updating: Reduction and quantification of uncertainties," Ph.D. dissertation, Faculty of Civil Eng., Bauhaus University, Weimar, Germany, 2011.
[26] A. Oktav, "Determination of the effect of adhesive fillets and viscous damping on the dynamic response of aluminum honeycomb sandwich panels," *Mech. Adv. Mater. Struct.*, pp. 1−11, Sep. 2023.
[27] S.R. Keshavanarayana, H. Shahverdi, A. Kothare, C. Yang, and J. Bingenheimer, "The effect of node bond adhesive fillet on uniaxial in-plane responses of hexagonal honeycomb core," *Compos. Struct*., vol. 175, pp. 111–122, 2017.
[28] P. Kendall, M. Sun, D. Wowk, C. Mechefske, and I. Y. Kim, "Experimental investigation of adhesive fillet size on barely visible impact damage in metallic honeycomb sandwich panels," *Compos. Part B Eng*., vol. 184, 107723, 2020.
[29] M. Sun, D. Wowk, C. Mechefske, E. Alexander, and I. Y. Kim, "Surface and honeycomb core damage in adhesively bonded aluminum sandwich panels subjected to low-velocity impact," C*ompos. Part B Eng*., vol. 230, 109506, 2022.
[30] *Simcenter Nastran Basic Dynamic Analysis User's Guide, Simcenter 3D 2022.1 Series*, Siemens, 2022.
[31] A. Jensen and K. Hamilton. (2017). PSD random vibration analysis in FEMAP. [Online]. Available: https://www.predictiveengineering.com/support-and-training/whitepapers/FEA
[32] C. Lalanne, *Mechanical Vibration and Shock Analysis, Random Vibration*, John Wiley & Sons, Great Britain, and the United States by ISTE Ltd, 2013.